Earth and Planetary Science Letters 427 (2015) 215–225

Contents lists available at ScienceDirect

Earth and Planetary Science Letters

www.elsevier.com/locate/epsl

Constraints on the crystal-chemistry of Fe/Mg-rich smectitic clays on Mars and links to global alteration trends

Joseph R. Michalski [a,b,*], Javier Cuadros [a], Janice L. Bishop [c], M. Darby Dyar [d], Vesselin Dekov [e], Saverio Fiore [f]

[a] Dept. of Earth Sciences, Natural History Museum, London, SW7 5BD, UK
[b] Planetary Science Institute, Tucson, AZ, USA
[c] SETI Institute, Mountain View, CA, USA
[d] Mount Holyoke College, South Hadley, MA, USA
[e] Département Géosciences Marines, IFREMER, Plouzané, France
[f] University of Bari, Bari, Italy

ARTICLE INFO

Article history:
Received 13 January 2015
Received in revised form 18 May 2015
Accepted 13 June 2015
Available online 24 July 2015
Editor: C. Sotin

Keywords:
clays
clay minerals
Mars
infrared
astrobiology

ABSTRACT

Near-infrared remote sensing data of Mars have revealed thousands of ancient deposits of Fe/Mg-rich smectitic clay minerals within the crust with relevance to past habitability. Diagnostic metal–OH infrared spectroscopic absorptions used to interpret the mineralogy of these phyllosilicates occur at wavelengths of 2.27–2.32 μm, indicating variable Fe/Mg ratios in the clay structures. The objective of this work is to use these near infrared absorptions to constrain the mineralogy of smectites on Mars. Using Fe/Mg-rich seafloor clay minerals as mineralogical and spectroscopic analogs for Martian clay minerals, we show how crystal–chemical substitution and mixed layering affect the position of the diagnostic metal–OH spectral feature in smectitic clay minerals. Crystal-chemistry of smectites detected on Mars were quantitatively constrained with infrared data and categorized into four mineralogical groups. Possible alteration processes are constrained by comparisons of clay chemistry detected by remote sensing techniques to the chemistry of candidate protoliths. Of the four groups identified, three of them indicate significant segregation of Fe from Mg, suggestive of alteration under water-rich and/or oxidizing conditions on Mars. The fourth group (with low Fe/Mg ratios) may result from alteration in reducing or water-limited conditions, potentially in subsurface environments. Some samples are interstratified di–trioctahedral clay minerals that have characteristics of dioctahedral clay minerals but clear chemical evidence for trioctahedral sheets. Approximately 70% of smectite deposits previously detected on Mars are classified as Fe-rich (FeO/MgO > 10). Only 22% of detections are trioctahedral and relatively Mg-rich. An additional ~8% are difficult to characterize, but might be very Fe-rich. The segregation of Fe from Mg in Martian clay minerals suggests that Mg should be enriched in other contemporaneous deposits such as chlorides and carbonates.

1. Introduction

Near-infrared remote sensing data of Mars collected by two instruments, OMEGA (*Observatoire pour la Minéralogie, l'Eau, les Glaces et l'Activité*) and CRISM (Compact Reconnaissance Imaging Spectrometer for Mars), have revealed thousands of detections of ancient Fe/Mg-rich smectite clay minerals (in addition to other clay minerals) within the Martian crust (Poulet et al., 2005; Murchie et al., 2009; Ehlmann et al., 2011; Carter et al., 2013). These materials likely formed through aqueous chemical alteration of pyroxene, olivine, and mafic glass within volcanic and impact-fragmented materials (Christensen et al., 2001; Poulet et al., 2007). Because these clay minerals are key indicators of aqueous activity, they are of astrobiological interest and important for understanding the climate history of Mars (Bibring et al., 2006). Despite the fact that remotely detected Martian smectites are unlikely to be pure clay deposits, the spectra of the clay mineral components contain key information about their crystal chemistry and structure. However, the precise mineralogy of the Fe/Mg-rich smectites is not well understood, limiting the ability to connect these deposits to their protoliths through their geochemistry, or to understand the nature of aqueous processes from whence they formed on ancient Mars.

* Corresponding author at: Natural History Museum, London, UK.
E-mail address: j.michalski@nhm.ac.uk (J.R. Michalski).

http://dx.doi.org/10.1016/j.epsl.2015.06.020

Spectral variability of the Martian smectites observed in the wavelength region of 2.27–2.32 μm is related to the clay minerals' crystal chemistry (Bishop et al., 2002a, 2002b; Gates, 2005), suggesting variability from Fe-rich to Mg-rich compositional end-members (Carter et al., 2013). Smectitic clay minerals present a challenge because the spectral shift from 2.27 μm (Fe-rich) to 2.32 μm (Mg-rich) appears to be linear and continuous, suggesting a continuous compositional range between the two end-members. Yet, most previous clay mineralogy research has suggested that a continuous and perfect solid solution between the dioctahedral Fe^{3+}-rich smectite (nontronite) and the trioctahedral Mg^{2+}-rich smectite (saponite) does not exist (e.g., Grauby et al., 1994). Instead, intermediate compositions result from intimate structural mixtures of trioctahedral and dioctahedral domains (Grauby et al., 1994; Deocampo et al., 2009; Cuadros, 2010). The Fe–Mg–smectite-system is further complicated by the variable valence state of Fe and therefore, the relationship between Fe/Mg ratio in smectitic clay minerals and near-infrared spectral features (2.27–2.32 μm) is not well understood.

Many remotely detected Martian clay minerals are considered to be "smectitic" because, additional to the metal–OH spectral features described above, they generally exhibit a spectral absorption located at 1.91–1.93 μm related to adsorbed water (Poulet et al., 2005; Ehlmann et al., 2009). Adsorbed water is much more common in expandable clay minerals (smectites) than in non-expandable clay minerals (Madejova et al., 1994; Bishop et al., 1994). However, mixed layering between expandable clay minerals (smectites) and non-expandable clay minerals is common in nature (Cuadros, 2010) and therefore many clay minerals that exhibit smectitic properties are not 100% smectite. An example of such behavior is clear in the talc–saponite system, where mixed layering occurs between the expandable >10 Å-clay (tetrahedral–octahedral–tetrahedral, or TOT) saponite and non-expandable TOT clay, talc (~9.4 Å) (Cuadros et al., 2008). Similar scenarios are observed between expandable Fe-rich TOT clay (e.g. nontronite) and non-expandable Fe-rich TOT clay (e.g. glauconite) (Cuadros et al., 2013). In addition, water not only occurs at the grain surfaces and in the interlayer sites of smectite, but in the hexagonal cavity created by the tetrahedral sheets close to octahedral Fe atoms in non-expandable layers, where it is more strongly held than in the interlayer positions (Cuadros et al., 2008, 2013). The implication is that significant molecular water can also occur in clay minerals other than pure smectite. Therefore, there are a range of possibilities for crystal–chemical variation of Fe/Mg-rich smectitic clay minerals on Mars, ranging from pure chemical substitution among smectites to mixed layering between discreet sheets or layers of different compositions (e.g., Bishop et al., 2008; Milliken et al., 2010).

This paper builds upon previous works (e.g. Ehlmann et al., 2011; Carter et al., 2013) to further explore the mineralogy of Martian clay minerals, specifically Fe/Mg-rich smectitic clay minerals. We have analyzed Fe/Mg-rich clay minerals found within hydrothermal sediments obtained from terrestrial seafloor cores extracted from a number of basins around the globe, as well as some samples selected from subaerial continental settings. Mineralogical, crystal–chemical, and spectroscopic variations among this sample group place stricter constraints on the mineralogy of Martian Fe/Mg-rich smectites and their likely protolith compositions and alteration styles on Mars.

2. Materials and methods

2.1. Materials

Sea floor hydrothermal clay deposits were chosen as analogs because they are chemically variable over small scales (cm–dm) and contain smectites with a compositional range relevant to Mars (Fe- and Mg-rich). A large number of samples was collected from these materials, and subsequently down-selected to minimize the effects of non-phyllosilicate impurities on our interpretations of mineralogy and chemistry. The geographic origin, geologic context, mineralogy, and chemistry of most of the samples discussed here were reported previously (Cuadros et al., 2013). All of those samples were extensively characterized by X-ray diffraction (XRD), including quantitative modeling of interstratified clay minerals from XRD data, chemical analysis, thermal gravimetry-evolved gas analysis (TG-EGA), Mössbauer spectroscopy, scanning electron microscopy (SEM), and transmission infrared spectroscopy. In addition to the 32 samples from Cuadros et al. (2013), this paper includes three terrestrial nontronites (Sampor, SWa-1 and Gossendorf) (Bishop et al., 1999, 2002a).

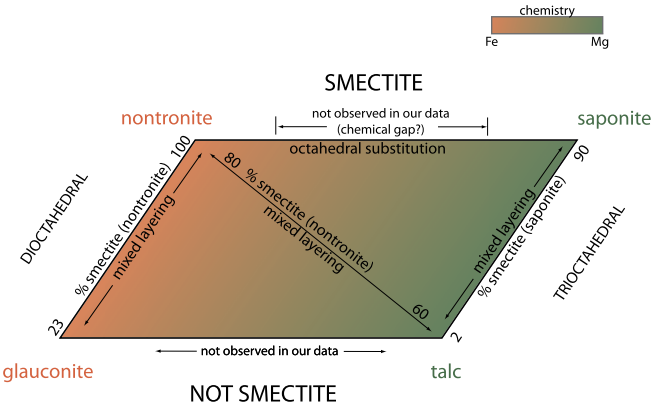

Fig. 1. The compositional range of samples used in this study is depicted graphically. Our samples span a range of crystal–chemical space between Fe- and Mg-end-members. Intermediate compositions occur because of both chemical substitution within sheets and due to mixed layering. The Fe-rich samples include nontronite and glauconite–nontronite mixed-layer clay minerals. The Mg-rich samples include talc–saponite mixed-layer clay minerals. Di–trioctahedral talc–nontronite is also observed. True intermediate solid solution between saponite and nontronite is not observed in our data.

In total, 35 well-characterized clay samples were selected for analysis by near-infrared spectroscopy in this work. Fig. 1 illustrates the mineralogical and chemical range of sample materials used here (see Cuadros et al., 2013 for more information, specifically Tables 2 and 4, and supplementary information). The samples span compositional space in the Fe–Mg system due to chemical substitution and mixed layering. For example, Mg^{2+} occurs in the dioctahedral sheets of nontronite and can substitute for Fe^{3+}. Likewise, Fe^{3+} can substitute for Mg^{2+} or Fe^{2+} within the octahedral sheets of saponite, as observed in our data; such substitutions are generally charge-balanced by vacancies. Complete solid solution between the two end-member compositions is lacking, and there is a chemical gap where true intermediate chemical substitutions are not observed.

Interstratification or mixed layering is observed in multiple variations in our samples. Mixed layering is observed between nontronite and glauconite, between talc and saponite, and between talc and nontronite (Fig. 1). Talc–saponite (T–S) spans the greatest range of ratio between expandable and non-expandable clay minerals (T–S from 10–90 to 98–2). Glauconite–nontronite (G–N) spans a range from 23–77 to 68–32. There is also evidence for mixed layering between talc and nontronite (T–N), where the ratios of mixing occur over a smaller range (T–N from 20–80 to 40–60). This subset of samples (T–N), referred to as di–trioctahedral in this paper, is interesting because it represents interstratification between trioctahedral and dioctahedral layers. However, in addition to mixed layering or interstratification, there is evidence of dioctahedral domains within trioctahedral sheets

and the opposite may also be true to a lesser extent (Cuadros et al., 2013).

2.2. Methods

Details of the characterization procedures used here are identical to those described by Cuadros et al. (2013). In summary, salts were first washed out of the samples and the <2 μm or <4 μm fraction was separated, where necessary, to avoid insoluble contaminants. Clay minerals were then characterized by XRD, wet chemical analyses, Mössbauer spectroscopy, TG-EGA, and mid-infrared (MIR) transmission spectroscopy. This study includes characterization by the additional technique of near-infrared (NIR) reflectance spectroscopy and connection to relevant aspects of the MIR.

Well-characterized clay mineral powders (the samples analyzed by Cuadros et al., 2013) were analyzed by infrared reflectance spectroscopy at the Keck-NASA RELAB facility at Brown University. Approximately 100 mg of each sample was prepared as a loose powder in a 1-cm diameter sample cup. Spectra were collected over a wavelength range from 0.8 to 100 μm under a nitrogen purge after equilibrating overnight. The spectral range of most interest was from 2.15 to 2.40 μm, where a spectral resolution of 2 cm^{-1} equates to ~1 nm. Through a series of trials, the samples were measured under both purged and ambient conditions, with no observable differences in this part of the spectrum.

In the 2.15–2.40 μm spectral range, vibrational absorptions correspond to metal–OH combination bands (combinations of the OH bending and stretching fundamentals) (Farmer, 1974). In another study (Cuadros et al., in review) we describe a procedure for fitting Gaussian curves to these hydroxyl bands to evaluate the contribution from individual bond types to the overall spectral character of each clay sample (Cuadros et al., in review). In this work, we simplified the procedure and extracted the wavelength position of the absorption maximum (reflectance minimum) in the region where metal–OH absorptions occur (2.27–2.32 μm). In reality, the absorption strength and position of this band is a complex function of overlapping Fe_2OH, FeMgOH, Mg_3OH and possibly Mg_2FeOH and/or $MgFe_2OH$ absorptions. In Fe/Mg-rich smectites, all of these components contribute to the character of one strong combination band that is diagnostic of clay chemistry in this range. It is important to note that the position of this absorption is directly comparable to reflectance spectra from CRISM and OMEGA. However, the error in resolving the wavelength of the absorption maximum in laboratory data is approximately 1 nm in this case, and the comparable uncertainty for CRISM is approximately 6.5 nm.

To compare laboratory results to reflectance spectra of Mars from CRISM, we extracted spectra from 30 different clay-bearing localities on Mars, allowing us to evaluate terrains that are dominantly smectitic in nature rather than those that likely contain chlorite (e.g. Milliken et al., 2010), serpentine, etc. (Appendix Table 1). The 30 regions of interest (ROIs) include several categories of geologic context: layered Hesperian–Noachian crust, layered materials in chaotic terrains, deep crust exposed in canyon walls or by erosion, crater rims and ejecta, and deep crust exhumed in the central peaks of impact craters. The average number of CRISM pixels per ROI is 1228, which equates to ~0.4 km^2/ROI, although this value includes one large outlier; the typical ROI size is ~0.2 km^2.

The goal in analyzing these 30 ROIs was to relate the spectral variability we observe in our lab data to the spectral variability that is observed among smectites on Mars using CRISM. The ROIs are not meant to be statistically representative of the total number of detections of smectites on Mars. Spectra from the 30 ROIs allow us to show how our lab data can be used to evaluate and classify CRISM spectra. In the discussion of this paper, we extend our analysis further to evaluate a statistically representative global dataset (Carter et al., 2013).

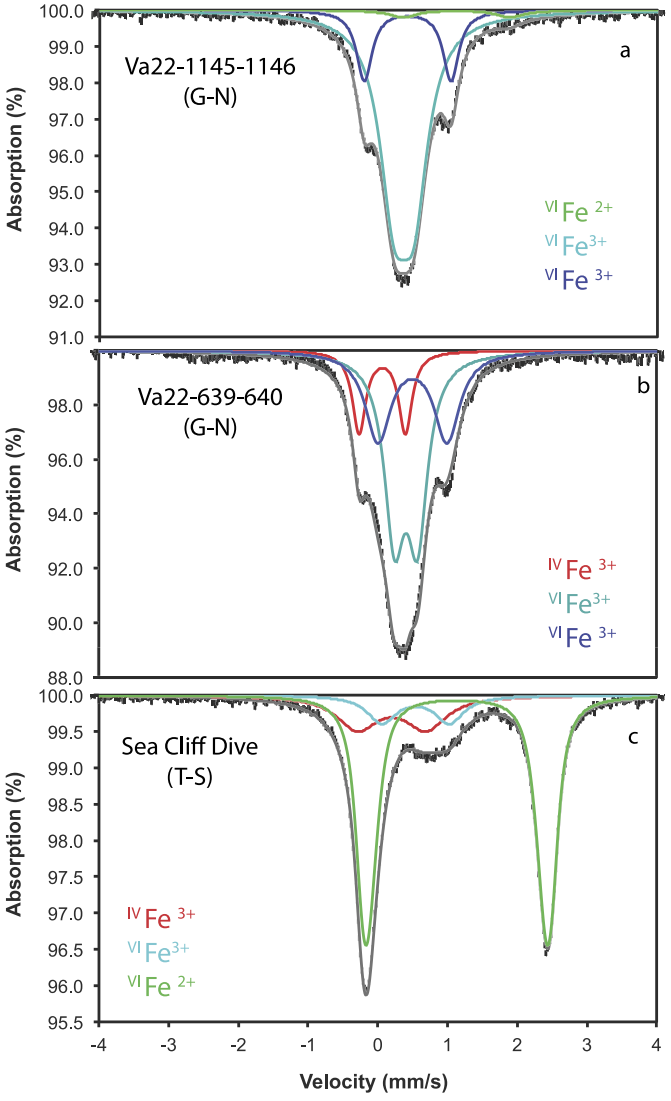

Fig. 2. Mössbauer spectra show three major categories of clay minerals in our sample suite. These include clay minerals with significant amounts of VI-coordinated Fe^{3+} occurring in the octahedral sheets (a), those with significant amounts of IV-coordinated Fe^{3+} in the tetrahedral sheets (b), and those with significant amounts of VI-coordinated Fe^{2+} in the octahedral sheets (c).

CRISM spectra were processed through the standard data pipeline to produce atmospherically corrected I/F data (Murchie et al., 2009). We extracted I/F data from regions of interest in each scene where clay signals were observed. The details of which scenes were used, number of pixels, and *X*, *Y* location in each scene are reported in Appendix Table 1. The extracted spectra were continuum-corrected in the wavelength range from 2.1 to 2.6 μm for comparison to the continuum-corrected lab data.

3. Results

3.1. Clay mineralogy and crystal-chemistry

The combined results from XRD, chemical analysis, TG-EGA, and Mössbauer spectroscopy provide strong constraints on the actual crystal-chemistry of the samples (Cuadros et al., 2013). The Mössbauer results in particular provide key information required for relating the infrared absorptions to Fe^{3+} and Fe^{2+}-content. Fig. 2 shows three key examples of Mössbauer spectra for our samples.

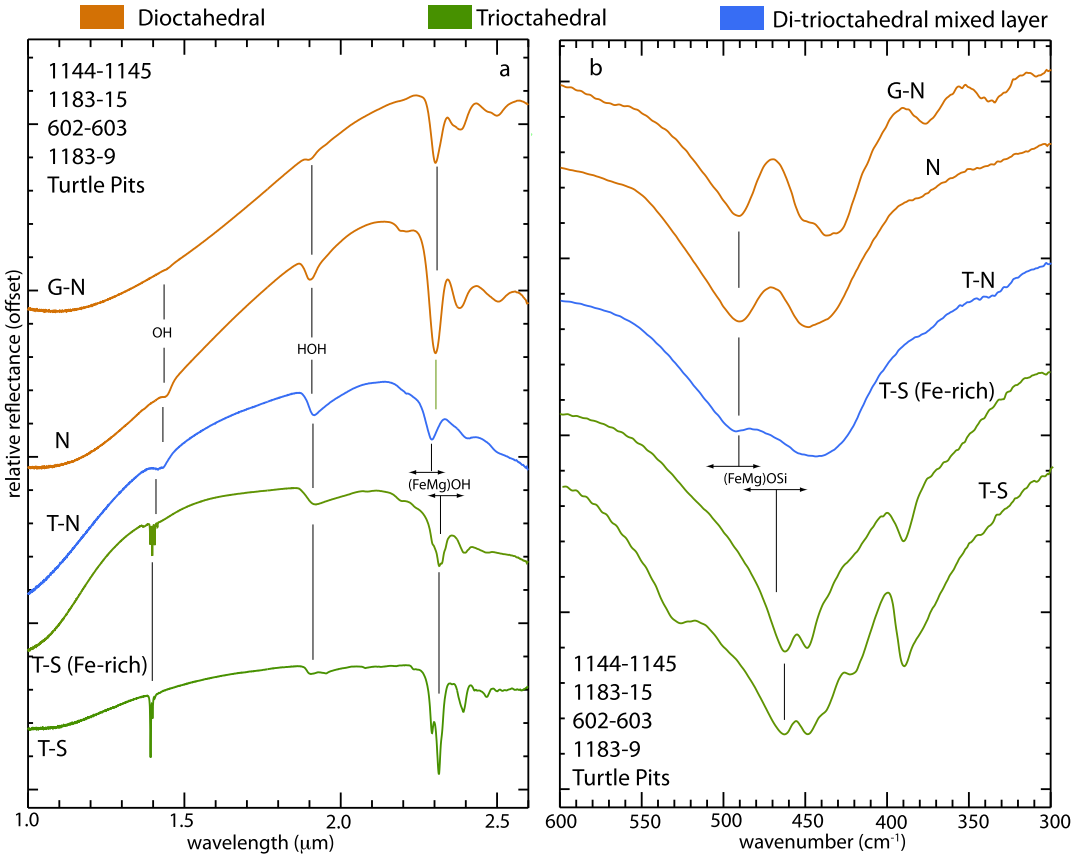

Fig. 3. Near-infrared reflectance and mid-infrared transmission spectra (scaled and offset) are shown for five different sample types. These include glauconite–nontronite (G–N), nontronite (N), talc–nontronite (T–N), Fe-rich talc–saponite and talc–saponite (T–S). Sample labels, in the same order from top to bottom, correspond to these five samples as described by Cuadros et al. (2013). The two main NIR spectral features of interest in this work are the metal–OH features related to octahedral Fe and Mg located near $\lambda = 2.27$–2.32 μm and the feature related to adsorbed or interlayer water located at $\lambda = 1.91$–1.93 μm (a). Mid-infrared transmission spectra are shown at the right (b). The key absorption of interest here is a metal–O–Si absorption that can be used to interpret clay compositions on Mars from thermal infrared data (Michalski et al., 2010).

One important result is the distinction between Fe^{3+} in tetrahedral versus octahedral environments. Some of our samples contain large amounts of tetrahedral Fe (e.g. Va3-150–153, a T–N sample with 23% of the Fe occurring as $^{IV}Fe^{3+}$) even if Al is present (though Al is in very low abundance in general) (Fig. 2). A second important result is the distinction between 6-coordinated Fe^{3+} and Fe^{2+} in the octahedral sheets. Our samples contain moderate amounts of Fe^{2+}, especially in the Fe-rich talc samples, but also in glauconite–nontronite and talc–nontronite mixed-layer clay minerals (Fig. 2). Lastly, the Mössbauer data were used to identify Fe^{3+} in multiple 6-coordinated environments, including multiple sites in clay minerals (Drits et al., 1997), and in oxyhydroxide, and oxide contaminants, if present. With these data, we were able to avoid samples with contamination or correct for minor contamination if present.

3.2. Infrared results

Near-infrared reflectance spectra of our samples show all of the typical features of clay minerals in the range from 1 to 2.6 μm (Fig. 3), including OH stretching overtones near 1.4 μm, HOH stretching overtones associated with bound and interlayer water at 1.41 μm, HOH combination stretching plus bending vibrations due to bound and interlayer water at 1.91 μm, and OH combination bands at 2.28–2.32 μm. In general, the Fe^{3+}-rich, dioctahedral clay minerals absorb at lower wavelengths (~2.28–2.29 μm) compared to the Mg-rich smectite, talc and talc-smectite (2.31–2.32 μm). This general observation is not surprising (e.g., Bishop et al., 2002a), but the details are in fact interesting and revealing. When the wavelength of the FeMgOH combination band is plotted against crystal-chemistry, several trends are revealed (Fig. 4).

Among the dioctahedral clay minerals (pure nontronite and glauconite–nontronite), there is a clear correlation between chemistry and position of the main metal–OH band (Fig. 4a). Most of these are of submarine origin, though a few are from non-marine settings (only those with the lowest wavelength absorptions, ~2.285 μm, are non-marine). The non-marine samples have primarily Fe^{3+} and Al^{3+} in the octahedral sheets and little or no Mg^{2+} or Fe^{2+}. Among all of our dioctahedral samples, increasing substitution of Fe^{2+} and Mg^{2+} up to 20% of the octahedral cations (Fig. 4c) consistently shifts the absorption maximum to longer wavelengths ca. 2.305 μm ($R^2 = 0.96$).

What causes the systematic shift? Because the shift occurs toward longer wavelengths (lower energies) with increasing substitution, it is likely that the substitution of divalent cations into the octahedral sheet results in an overall increase in the bond lengths involved. This could explain the systematic shift in our data. However, there is evidence that substitution into vacancies could actually decrease the bond length (Perdikatsis and Burzlaff, 1981). Further work is needed to determine exactly where the substitution occurs in the octahedral sheets.

The trioctahedral and di–trioctahedral mixed-layer clay minerals are complex (Fig. 4b). Substitution of trivalent cations for divalent cations should decrease the average bond lengths and therefore result in systematically shorter wavelength absorptions with increased Fe^{3+}- or Al^{3+}-content. But, we observed the contrary in our data. In the trioctahedral group (talc and talc–saponite), the position of the metal–OH combination band is only weakly corre-

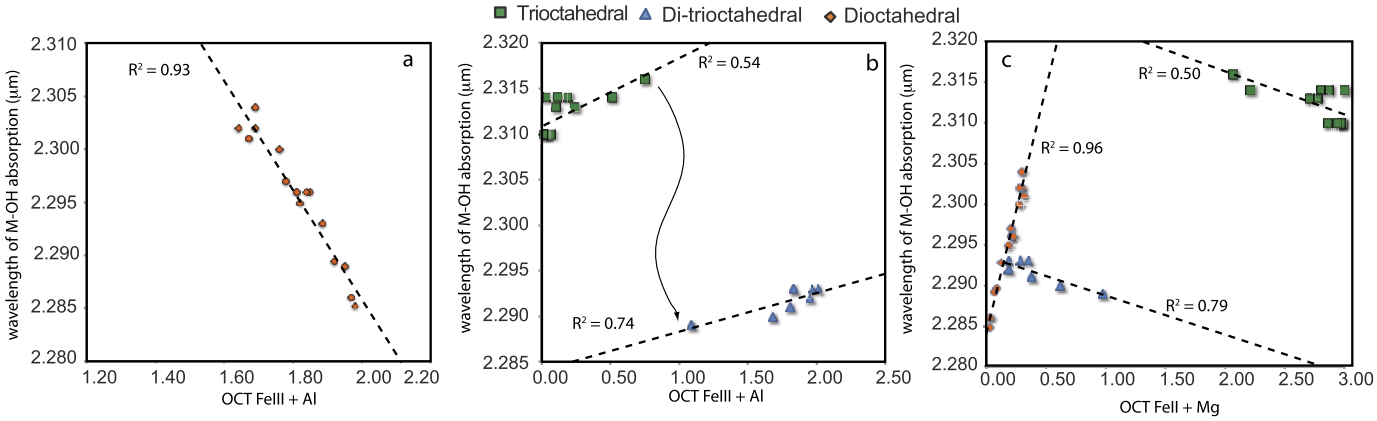

Fig. 4. Effects of octahedral sheet chemistry on the position of metal–OH combination bands. The wavelength of the Fe/Mg–OH absorption maximum (reflectance minimum) in smectitic clay minerals is compared to crystal chemistry of the samples: octahedral trivalent cations (Fe^{3+} and Al^{3+}) (a–b) and octahedral divalent cations (Fe^{2+} and Mg^{2+}) (c). The arrow in panel b shows an important spectral shift that occurs in trioctahedral sheets: increasing substitution of Fe^{3+} causes the metal–OH band to shift to longer wavelengths in trioctahedral and di–trioctahedral clay minerals but there is a wavelength gap between the two ranges. The reasons for this shift are discussed in the text and by Cuadros et al. (in review).

lated with Fe^{3+} and Al^{3+} content ($R^2 = 0.54$) or Fe^{2+} and Mg^{2+} content ($R^2 = 0.50$). For trioctahedral and di–trioctahedral samples, the addition of Al^{3+} and Fe^{3+} displaces the band position toward longer wavelengths, as seen in the positive slope in Fig. 4b.

This relationship among trioctahedral clay minerals might be understood in terms of the competing effects related to the nature of various fundamental bands contributing to the combination bands investigated here. Specifically, in trioctahedral clay minerals, increasing substitution of trivalent cations shifts the bending fundamentals to lower wavelengths and the stretching fundamentals to higher wavelengths. In the resulting combination, these effects are in conflict and the correlation between band placement and crystal-chemistry is weaker. However weak the correlation, the resulting combination band does shift toward higher wavelengths with increasing trivalent cations (Fig. 4b) or lower wavelength with increasing divalent cations (Fig. 4c).

Perhaps even more complicated are the di–trioctahedral clay minerals. These samples represent mixed-layer clay minerals with characteristics of both dioctahedral and trioctahedral clay minerals (Cuadros et al., 2013). In the NIR, the di–trioctahedral clay minerals are generally spectroscopically similar to dioctahedral clay minerals (Fig. 3a), but in the MIR, they are spectrally intermediate between the two (Fig. 3b). In the 400–550 cm^{-1} region, dioctahedral clay minerals exhibit a well-defined doublet that is not well-defined in trioctahedral clays (Fig. 3b). In this region, di–trioctahedral clays have a feature that is intermediate between dioctahedral and trioctahedral clay minerals, but they also exhibit well-developed bands associated with dioctahedral and trioctahedral clay minerals in the bending and stretching regions (not shown). In the NIR, their metal–OH combination band in di–trioctahedral clays occurs at 2.29–2.295 µm, similar to nontronite (Fig. 4c). In detail, the negative slope of the trend with increasing Fe^{2+} and Mg^{2+} content (Fig. 4c) mimics that of the trioctahedral clay minerals, reflecting the fact that true trioctahedral domains (i.e. occupancy >2.5 per $O_{10}[OH]_2$) are present. Here the wavelength of the composite band is a function of the varying contributions from each layer type and their overall bond length.

Fig. 4b highlights a major spectral shift where the wavelength of the metal–OH feature changes from ~2.315 µm to ~2.290 µm once trivalent cations (Fe^{3+} and Al^{3+}) reach a similar proportion to divalent cations (Fe^{2+} and Mg^{2+}). In trioctahedral clay minerals, the substitution of trivalent cations, especially Fe^{3+}, has the effect of increasing the wavelength of the metal–OH absorption, as described above and seen in Fig. 4b. As Fe^{3+} increases, unique nontronite-like domains form in the trioctahedral layers. Eventually, with increasing substitution, discreet dioctahedral sheets and layers form, resulting in a true di–trioctahedral mixed-layer clay (Cuadros et al., 2013). This shift has a profound effect on the position of the metal–OH combination bands (Fig. 4b).

Finally, spectra of Fe-rich talc can appear similar to smectite spectra. One of the talc–smectite samples (Turtle Pits in Fig. 3), with 21% saponite, has a strong and well-defined doublet at 2.31 µm, which is typical for Mg-rich, well-ordered talc. In contrast, the Fe-rich T–S sample (1183–9), with only 2% saponite, has a poorly defined doublet reflecting the less ordered nature of the talc, which is typical for Fe-rich talc (Cuadros et al., 2008). However, while the combination bands become more subdued in Fe-rich talc due to higher Fe-content, the overtone bands at 1.41 µm become much more complex. As might be expected, this mimics the behavior of Mg_3OH, Mg_2FeOH, $MgFe_2OH$, and Fe_3OH bands in Fe-rich talc at ~2.7 µm (Wilkins and Ito, 1967; Petit et al., 2004; Petit, 2005; Cuadros et al., 2008).

3.3. Mars remote sensing results

Each of the NIR spectra of the 30 surfaces analyzed contains an absorption at one of the CRISM band passes between 2.278 µm and 2.318 µm. Those absorptions are indicative of the Fe- and Mg-rich nature of the smectitic deposits on Mars and because they span the same spectral range (~2.28 µm and 2.32 µm) that we show in Fig. 4 for laboratory data, it stands to reason that the Martian smectites exhibit a similar compositional range. As is the case with the laboratory data, we can interpret the crystal chemistry of the Martian smectites in detail based on the precise position of these absorptions. These results are discussed further in the discussion section because they make more sense in the context of our classification scheme explained for our laboratory data below.

4. Discussion

4.1. Intermediate compositions of Fe/Mg-rich smectites

One of the measurables of Fe/Mg-rich smectitic clay minerals is the position of the metal–OH combination band. This absorption occurs between 2.27 and 2.32 µm and is the key indicator of clay mineralogy on Mars. CRISM spectra of clay-bearing rock units on Mars exhibit absorptions at several different wavelength positions from 2.27–2.32 µm. Is that an indication that smectite clay minerals on Mars exhibit true solid solution between Mg-rich and Fe-rich end-members in this range? If so, it would be surprising

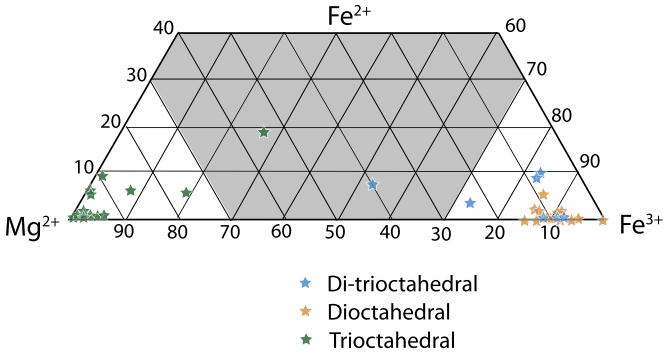

Fig. 5. The molar chemistry of the octahedral sheets of our sample is shown in ternary form. The gray area corresponds to intermediate compositions that are rare in nature. The position of the FeMgOH combination band shifts continuously between the Fe-rich and Mg-rich end-member positions, but yet our samples do not exhibit pure solid solution.

because FeMg-smectites do not commonly occur in solid solution on Earth (Deocampo et al., 2009); intermediate compositions more typically imply the existence of both dioctahedral and trioctahedral domains either within individual sheets (Grauby et al., 1994) or in interstratification of sheets (mixed layering) (Cuadros, 2010). Therefore the questions addressed below are: how do the chemistry of Fe/Mg-rich smectites relate to their NIR features? And, how can we interpret the chemistry of smectitic Fe/Mg-clay minerals on Mars from NIR data?

Fig. 5 is a ternary plot of the octahedral chemistry of our samples showing their relative abundances of Fe^{3+}, Fe^{2+} and Mg^{2+}. The plot shows that few of our samples truly exhibit intermediate compositions. In fact, most of the samples of nontronite, glauconite–nontronite, and di–trioctahedral mixed-layer clay minerals fall into a narrow, Fe^{3+}-rich zone. Likewise, the talc–saponite clay minerals are constrained to a relatively limited Mg-rich zone (Fig. 5). Only a few samples seem to have intermediate compositions. These are the very Fe-rich talc sample (1183–9) and a complicated sample, nontronite 51, which is a talc–nontronite that includes a small amount of talc physically mixed in addition to mixed layering. Our geochemical results support the idea that true chemical solid solution between Mg- and Fe-rich smectites is uncommon in nature (see "chemical gap" in Fig. 1) (Grauby et al., 1994).

While the geochemistry of our samples does not seem to be truly linear between Fe- and Mg-rich end-members, it is true that we generally see a spectral continuum between the Fe-rich side (~2.28 μm) and the Mg-side (2.32 μm). The middle ground (clay minerals that absorb from 2.29 to 2.305 μm) is occupied by relatively Mg-rich dioctahedral clay minerals, and to some extent, by di-trioctahedal clay minerals (Fig. 4c). Those dioctahedral clay minerals are common on Earth and, as described below, they are critically important for understanding clay minerals on Mars. The di–trioctahedral clay minerals are more complicated and less common, but also important on Mars.

4.2. Classification of smectitic clay minerals from spectral data

One of the goals of this work has been to categorize Fe/Mg-rich smectite clay minerals in a way that is applicable to Martian remote sensing data and useful for geological interpretations. In categorizing the data, we focused on the Fe/Mg ratio of the clays, as this provides a geochemical distinction that can be understood in the context of the most common types of chemical analyses of other Martian materials. In doing so we lose the distinction between Fe^{2+} and Fe^{3+}, which is relevant spectroscopically, but which is also difficult to establish accurately in remote sensing analysis of Mars surface. Moreover, while Martian smectitic clay minerals might have formed with appreciable Fe^{2+} on their structures, it is possible that Fe^{2+} would be oxidized to Fe^{3+} in clays exposed to the Martian atmosphere. Therefore, grouping of Fe^{2+} and Fe^{3+} into "total Fe" for smectitic clay minerals on Mars is likely a reasonable assumption.

To distinguish clay minerals according to their Fe/Mg ratios, we considered two systems: the first is with regard to molar octahedral chemistry (Fig. 6a) and the second to total sample chemistry

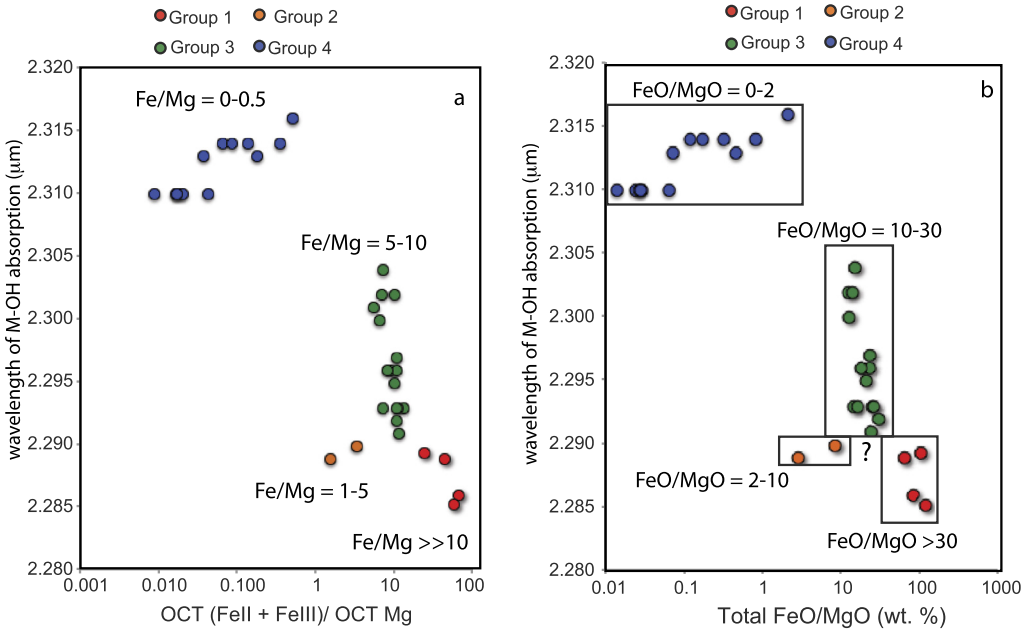

Fig. 6. Fe–Mg-rich smectitic clay minerals can be categorized into four chemical groups based on near-infrared data. Panel a shows the position of the absorption maximum of the metal–OH combination band plotted against molar octahedral crystal chemistry. In panel b is the same type of plot, but where the chemistry represents bulk sample FeO and MgO. Note that all Fe_2O_3 was recast as FeO in this plot. The four groups are discussed in the text. Note that the group order can be confusing because the FeO/MgO decreases in the order: Group 1, 3, 2, and 4 whereas the spectral positions decrease in the order of the group numbers. Group 1 is very high FeO/MgO and Group 2 is low-moderate FeO/MgO, but these two groups can be difficult to distinguish in the infrared based on complex Fe-substitution and mixed layering (see Fig. 4c).

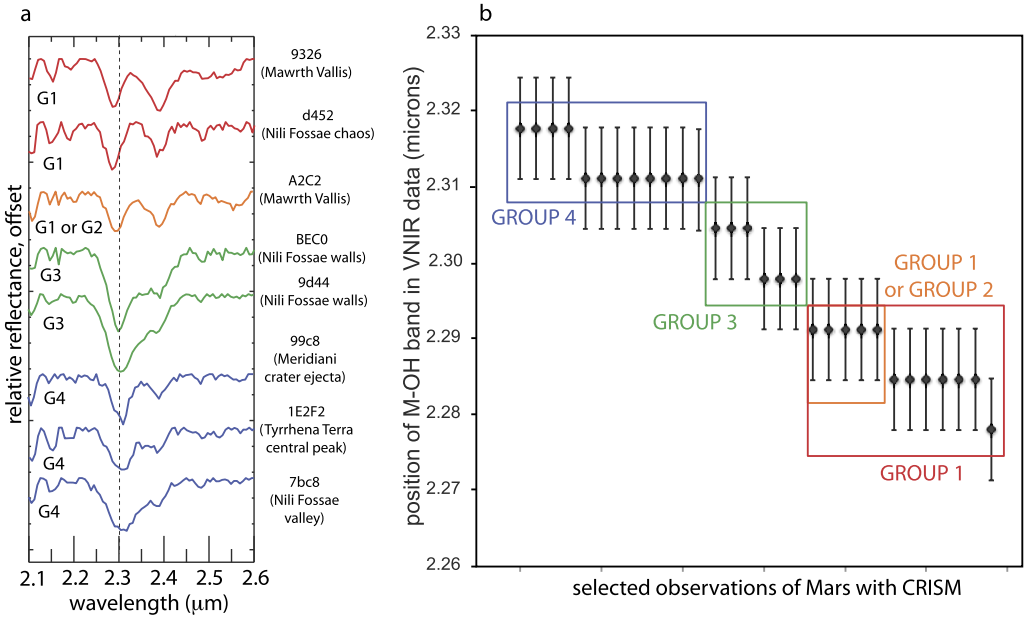

Fig. 7. CRISM spectra of smectitic clay minerals were extracted for 30 deposits representing a range of contexts on Mars. Examples of spectra from each group are shown in panel a. The absorption maximum of the FeMgOH combination feature in each continuum-corrected I/F spectrum is plotted for each deposit, showing the range of compositions of Fe/Mg-rich smectitic clay minerals on Mars (b). These are categorized into groups using the breakdown in Fig. 6b. Note that these spectra are meant to represent most of the range of spectral variability among FeMg-smectites on Mars, not a statistical representation of the actual frequency of occurrence.

(MgO and FeO) (Fig. 6). Note that FeO in this case corresponds to total Fe because all Fe_2O_3 is recalculated as FeO. Ultimately, we chose the latter system (FeO v. MgO) because it is more relevant to our goal of relating the clay geochemistry to possible Martian protoliths, most of which are evaluated in terms of total Fe reported as FeO.

Fig. 6 relates the spectral position of the metal–OH combination band to the octahedral chemistry of the clay minerals and the total Fe-content of our sample group. Based on the combined spectral variation and chemistry of samples, we categorized the materials into four groups. Whether one views the data in molar or oxide-space (Fig. 6a or 6b), there are three obvious distinctions: very low Fe/Mg ratio, moderate Fe/Mg ratio and very high Fe/Mg ratio. Despite this natural cluster into three groups, we defined an additional fourth group that corresponds to materials with unusual Fe/Mg ratios versus spectral character. These correspond to di–trioctahedral clay minerals that have interesting spectral character, as described above.

Here we describe the grouping based on total FeO/MgO, as illustrated in Fig. 6b. Group 1 clay minerals are those with very high FeO/MgO ratios (>30). These correspond to non-marine nontronites and low-Mg submarine nontronites that have combination bands at 2.28–2.29 μm. Group 2 is the anomaly in the sense that it exhibits highly variable Fe/Mg ratios and it does not fit the trend of Groups 1, 3 and 4. Group 2 includes the clay minerals that have spectral features that overlap with those of Group 1 (features located at ∼2.29 μm), but have very different FeO/MgO ratios (2–10 for Group 2 versus >30 for Group 1). As described above, this overlap occurs due to complex attributes of the trioctahedral combination bands (Cuadros et al., in review) and the complex effects of chemical substitution and mixed layering between trioctahedral and dioctahedral sheets. Group 3 includes a range of smectitic samples (mostly dioctahedral, but also di–trioctahedral clays) that are Mg-bearing, but generally Fe-rich (FeO/MgO ∼10–30). Finally, Group 4 clay minerals are trioctahedral clay minerals with relatively low FeO/MgO ratios (0–2). Note, however that most of these samples have an FeO/MgO ratio <1, and only one of them has a value of ∼2.

CRISM data extracted from smectite-bearing terrains on Mars can be compared to our lab data and also categorized into groups. However, in the case of the CRISM data, there is of course only the infrared band position available without the corresponding chemistry. Fig. 7a shows examples of extracted CRISM spectra corresponding to each group. Fig. 7b shows the wavelength of the metal–OH combination band for all 30 terrains analyzed. Similar to the classification of laboratory spectra, the CRISM spectra can be categorized into the four groups based on the position of the metal–OH absorption. Note that Group 2 cannot actually be identified uniquely because it (spectroscopically) falls within Group 1, but it is important to point out that this group could exist on Mars, especially given the evidence for clays that appear to be trioctahedral but very Fe-rich (Michalski et al., 2010).

4.3. Global occurrences of smectitic clay classes

Our analysis of CRISM data for 30 ROIs is meant to illustrate the range of smectitic compositions on Mars based on the position of the metal–OH band. Those results (Fig. 7) were not intended to be a statistically complete representation of the number of occurrences or detections of smectites on Mars. However, it is possible to apply our classification of smectitic clays to a global dataset, which is statistically representative with regard to number of detections of smectitic clays.

Carter et al. (2013) performed an exhaustive analysis of the occurrence of clay minerals on Mars using OMEGA and CRISM data. Using Carter's database of >1000 detections of smectites on Mars (we used 1007 of those data points), we classified each detection into one of Groups 1–4 based on the position of the metal–OH absorption in the 2.27–2.32 μm spectral range. In other words, the classification scheme demonstrated in Fig. 7 can be applied to a large, global database of Martian smectitic clays. Fig. 8a shows the results of this classification for each of the 1007 smectite detections from the database of Carter et al. (2013) overlaid on geologic surface age. There are several observations to note: 1) the smectites occur almost entirely in Noachian terrain, considering the most recent global geologic surface mapping (Tanaka et al., 2014), 2) the most common group of smec-

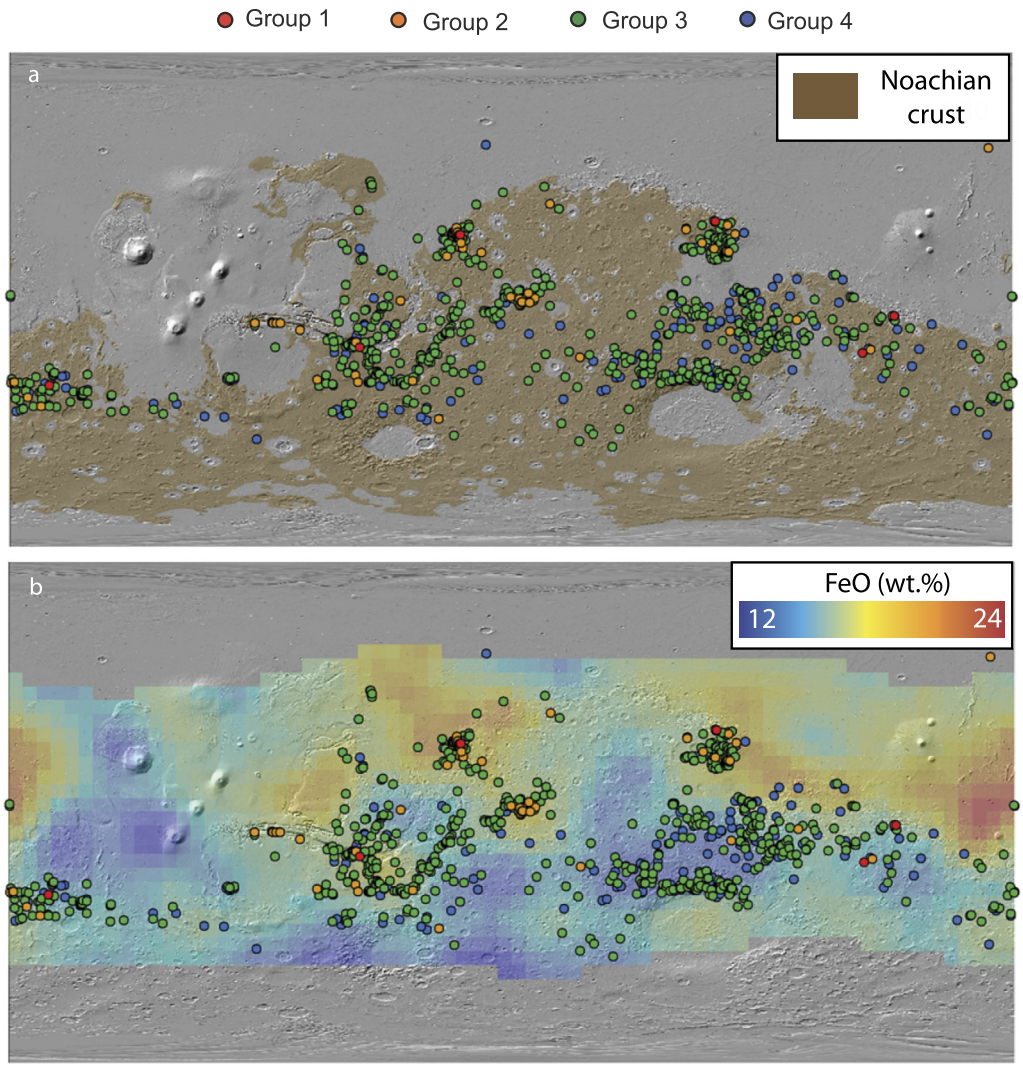

Fig. 8. Global classification of smectitic clays on Mars. We used the global database of Carter et al. (2013) to classify the composition of 1007 Fe/Mg-rich smectite detections on Mars according to our four groups described in the text. Smectite detections are overlaid on Noachian geologic surface ages (Tanaka et al., 2014) (a) and on Fe (converted to FeO) abundance detected by GRS (Boynton et al., 2008). Clay groups, which are categorized by Fe-content, are decoupled from crustal FeO-content, as derived by GRS.

titic deposit corresponds to Group 3 – very Fe-rich clay minerals, and 3) there is no clear spatial correlation among the groups.

Considering that our classification of clay minerals on Mars is focused on Fe-content, it makes sense to compare the geographic occurrence of different groups to the Fe-content of the Martian crust, as observed in Gamma Ray Spectrometer (GRS) data (Boynton et al., 2008) (Fig. 8b). While some Fe-rich clay mineral deposits occur within Fe-rich terrains, they also occur in relatively Fe-poor terrains; there is no obvious correlation between bulk crust composition (GRS integrates surface chemistry measurements over the uppermost decimeters) and clay composition in the NIR (which is sensitive to the uppermost ~10 s–100 s of μm).

The global results reveal important insights into the chemistry of Martian clay minerals (Fig. 9). Most strikingly, the results show that 69% of all detections of smectitic clay on Mars correspond very Fe-rich (FeO/MgO = 10–30) dioctahedral and di–trioctahedral clay minerals (Group 3), described in detail in Section 4.1 above (Fig. 9). Approximately 22% of the smectitic clay minerals detected on Mars fall into the trioctahedral, relatively Mg-rich category. Only ~1% of the total would fall into Group 1, which are extremely Fe^{3+}-rich, Mg^{2+} and Fe^{2+}-poor dioctahedral clay minerals. The remaining 8% is difficult to characterize (Group 2). These are clay minerals that, based on their infrared characteristics, might

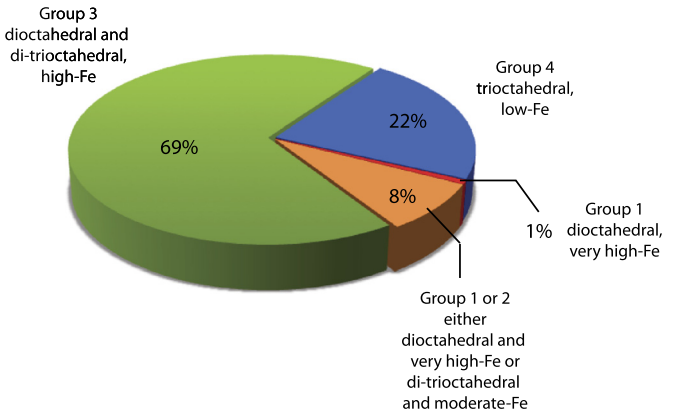

Fig. 9. The actual abundance of each group of smectitic clay on Mars. Carter et al. (2013) described the global occurrences of smectitic clay minerals on Mars from CRISM data, and counted the number of occurrences of clay minerals based on metal–OH absorptions at each wavelength in the metal–OH combination region (2.27–2.32 μm). Here we categorize those results according to our crystal–chemical groups. Only 22% of the smectite occurrences are relatively Mg-rich. Most (70% – Groups 1 + 3) are very Fe-rich (FeO/MgO > 10). An additional 8% corresponds to di–trioctahedral clay minerals of moderate FeO/MgO or possibly to very high-Fe dioctahedral clay minerals.

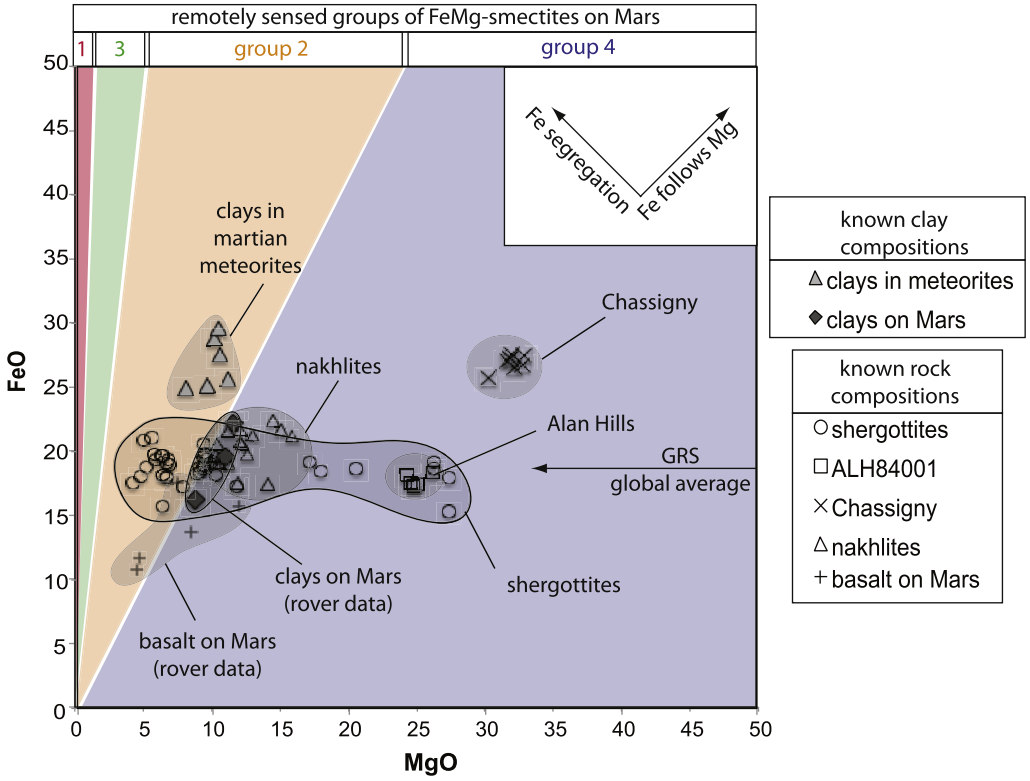

Fig. 10. A comparison of the known bulk FeO/MgO ratios of Martian materials compared with the FeO/MgO ranges interpreted from infrared data. The colored ranges correspond to spectral Groups 1–4 as defined in Fig. 6b (note that the group order is intended to progress from 1 to 3 to 2 to 4 in terms of FeO/MgO ratio). The point data correspond to 157 analyses of: Martian meteorites (bulk chemistry), compositions of Martian clay minerals measured within Martian meteorites, compositions of igneous rocks on Mars measured by rovers, and compositions of clay deposits on Mars measured by rovers. Note that most Martian clay deposits detected remotely (Fig. 8) have higher FeO/MgO ratios than most Martian igneous compositions, suggesting significant Fe segregation by aqueous alteration processes.

be either di–trioctahedral and somewhat Fe-rich or purely dioctahedral and very Fe^{3+}-rich. To summarize, most of the smectites detected on Mars are Fe-rich and likely dioctahedral (nearly four-fifths). Only approximately one-fifth of the smectites detected on Mars are Mg-rich and trioctahedral (Fig. 9).

The notion that smectites on Mars are Fe-rich and complex (i.e. include mixed-layer varieties) is a reasonable one. Burns (1993) predicted the occurrence of complex Fe-rich smectites on Mars, even citing terrestrial analog samples from the Atlantis II Deep Basin, Red Sea (the setting where many of our samples were collected), as examples of such complex mineralogies. Such complex clay minerals could occur due to oxidation of Fe^{2+}-rich trioctahedral clay minerals, as described by Burns (1993), but they could also form if aqueous conditions on Mars were not stable and long-lived, because mixed-layer clay minerals form at phase boundaries and in kinetically inhibited conditions (Cuadros, 2010). The only clay minerals on Mars that are well understood through detailed, *in situ* analyses are those detected in Gale Crater by XRD with the Curiosity rover (Vaniman et al., 2013). These clays appear to be smectitic, trioctahedral and Fe-rich (compared to typical saponite) (FeO/MgO $\sim$ 2). No infrared data are available for the material because Curiosity does not carry any IR spectrometers. The closest chemical and structural comparison to these clay minerals is a trioctahedral smectite from Griffith Park, Los Angeles, USA (FeO/MgO = 0.7–1) (Treiman et al., 2014). This material clearly displays trioctahedral characteristics, and has NIR absorptions in the 2.308–2.315 μm range (Treiman et al., 2014), which places it in our Group 4. Therefore, the clays explored to date in the floor of Gale Crater might shed light on Group 4 clays detected on Mars from orbit.

4.4. Connections to protoliths and processes

One of the goals of this work is to make progress toward understanding the origin of smectitic clay minerals on Mars in terms of likely protoliths and aqueous alteration processes. Studies of Martian meteorites show how alteration of olivine can lead to formation of Fe^{2+}-rich saponite (TOT or 2:1 clay minerals), as well as TO (1:1) and 2:1:1 Fe/Mg-rich clay minerals (Changela and Bridges, 2010; Hicks et al., 2014). In those cases, the products and reactants are intimately texturally related and therefore, alteration products can be linked to protoliths. However, using remote sensing data, textural information is typically lost so it is generally impossible to link an exact protolith to an alteration product on Mars remotely.

Despite the limitations described above, it is possible to quantitatively constrain crystal-chemistry and bulk FeO/MgO ratios of smectitic clay minerals on Mars, and compare those constraints to known values for a range of possible protoliths. Fig. 10 plots the FeO/MgO ratios of known Martian materials compared to the chemical constraints for remotely sensed clays (Groups 1–4) (shown as colorized zones, based on chemical ranges of each group). The bulk chemistries of Martian meteorites are well known (Meyer, 2012). In addition, the chemistry of many igneous rocks have been measured *in situ* on the Martian surface with the Alpha Proton X-ray Spectrometers (APXS) aboard the Mars Exploration Rovers and Curiosity (McSween et al., 2009; Stolper et al., 2013). Lastly, we can consider, for the sake of comparison, the chemistry of clay deposits encountered by Mars rovers. These include clay minerals near Endurance Crater in Meridiani Planum analyzed by the Opportunity Rover (Arvidson et al., 2014) and clay minerals in Gale Crater (Vaniman et al., 2013). These data can be treated as "known compositions" because the rocks' chemistries

have been measured *in situ* and the chemical values are reliable. We can compare these known Martian rock and clay compositions to the compositional constraints of smectitic clay minerals on Mars based on our four composition groups described above. Of course, it is impossible to know the actual protoliths from which the remotely sensed clay minerals formed. But, known Martian rock compositions provide the best possible guidance. In Fig. 10, the color-coding by group represents the FeO/MgO compositional range for that group (e.g. Group 3 is bounded by lines of constant FeO/MgO ratio equating to 10 and 30).

An important conclusion from Fig. 10 is that Group 4 clays have similar compositions to most candidate igneous protoliths. The alteration processes that led to formation of Group 4 clays did not result in significant segregation of Fe from Mg. This could be an indication that such clays formed in water limited and/or reducing conditions. An example of such a setting might occur in rock-dominated subsurface environments, such as those settings proposed by Ehlmann et al. (2011) and Meunier et al. (2012). Alternatively, these clays might have formed in terminal deposits where Mg might be enriched (e.g. closed basin, terminal lakes) (Bristow and Milliken, 2011). Of course, the geologic setting of each clay detection must be evaluated independently, but this composition group is consistent with such provenance. However, Group 4 corresponds to only 22% of the smectite detections on Mars.

Another important conclusion from Fig. 10 is that most Martian smectitic clay deposits ($\geq$70%) are very Fe-rich compared to likely igneous protoliths. The alteration processes that formed clays in Groups 1 and 3 resulted in significant segregation of Fe from Mg. Such clays might have formed in settings that were water-rich and slightly oxidizing or less water-rich and extremely oxidizing. Such sites might correspond to surface environments or hydrothermal subsurface settings. Surface settings could include pedogenic alteration (e.g. Noe Dobrea et al., 2010; Gaudy et al., 2011). Subsurface settings might have included sustained hydrothermal environments in the shallow or deep crust (Ehlmann et al., 2009; Fairen et al., 2010). However, if these clays formed from subsurface fluids, those fluids were likely oxidizing enough to allow for segregation of Fe from Mg, which could implicate communication of the fluids with the surface environment.

The Group 2 clay minerals, which are complex di–trioctahedral phases, have compositions similar to some candidate protoliths and similar to clay minerals identified in Martian meteorites (e.g. Changela and Bridges, 2010). These deposits might represent transitional chemical environments and/or short-lived aqueous settings. They might also be relevant to clays on Mars that have NIR characteristics of Fe-rich dioctahedral clays, but thermal IR characteristics of trioctahedral clay minerals (Michalski et al., 2010).

A final consideration is the relationship of Fe-rich Martian clay minerals to other crustal materials (e.g. Milliken et al., 2009). A revised summary of global alteration on Mars, taking into account observational biases and biases due to dust cover, shows that much of the crust has been altered to clay minerals (Carter et al., 2013). Our results show that the smectites are largely very enriched in Fe relative to the likely protoliths, which suggests that Mg has been mobilized into other deposits. In this regard, it makes sense that most of the carbonates detected on Mars to date are Mg-rich (Ehlmann et al., 2008; Niles et al., 2013). In fact, Mg-rich carbonates are often observed together with Fe-rich smectites and were in many cases difficult to completely isolate from the Fe-smectite signatures (e.g. Ehlmann et al., 2009; Bishop et al., 2013). Likewise, it would not be surprising if ancient chloride deposits (Osterloo et al., 2010) are rich in Mg. Such a scenario makes sense if the formation of most clay minerals, chlorides and carbonates were roughly coeval on ancient Mars (Ehlmann et al., 2011) and predate the era in which water-limited, sulfate formation was dominant (Bibring et al., 2006).

5. Conclusions

We analyzed the near-infrared spectra of Fe/Mg-rich smectitic clay minerals in order to relate the crystal-chemistry of these clay minerals to their infrared features. Our results show good correlations between the crystal-chemistry of dioctahedral Fe/Mg-rich clay minerals and their spectral features. As Mg^{2+} and Fe^{2+} substitute into the octahedral sheets, the position of the combination band shifts predictably from lower wavelengths ($\sim$2.28 μm) to higher wavelengths ($\sim$2.30–2.31 μm). But, even at the higher wavelength end, the clay minerals are clearly Fe-rich. Trioctahedral clay minerals are more complicated. Substitution of trivalent cations into the octahedral sheet does not have as pronounced or predictable of an effect on the position of the relevant combination band. However, once a significant amount of substitution of trivalent cations is reached, complex di–trioctahedral clays form. The NIR metal–OH combination absorption in these di–trioctahedral clays is shifted dramatically to lower wavelengths compared to trioctahedral clays.

Based on our analyses of Fe/Mg-rich smectitic clay minerals in the laboratory, we categorized Fe/Mg-rich smectites observed on Mars by CRISM (Carter et al., 2013) into four groups. Most ($\geq$70%) of Martian smectitic clays are very Fe-rich (FeO/MgO $>$ 10). Only 22% of the smectite detections are relatively Mg-rich, trioctahedral clays. Therefore, compared to most known candidate igneous protoliths, Martian smectites are enriched in Fe.

In summary, the results suggest that ancient Martian smectitic clay minerals formed under conditions that generally favored segregation of Fe from Mg, though we cannot rule out the possibility that the clay minerals were originally Fe^{2+}-rich and subsequently became oxidized through exposure to the atmosphere (Burns, 1993). The geologic settings likely included both surface and subsurface environments. Segregation of Fe into clay deposits might suggest a systematic link between the formation of Fe-rich clay minerals and Mg-rich carbonates and/or Mg-bearing chloride deposits on ancient Mars.

Acknowledgements

This work was funded by a grant from the European Commission (Marie Curie Actions, “HYDROMARS”) and a grant from the UK Space Agency AURORA program (ST/L002078/1), both to the Natural History Museum, London. We wish to acknowledge John Carter for sharing his global dataset of spectral detections of smectites on Mars. Comments from two anonymous reviewers greatly improved the manuscript. We acknowledge RELAB and Takahiro Hiroi at Brown University for collecting near infrared data. We thank Caroline Smith for organizing meteorite data used in this work.

Appendix A. Supplementary material

Supplementary material related to this article can be found online at http://dx.doi.org/10.1016/j.epsl.2015.06.020.

References

Arvidson, R.E., et al., 2014. Ancient aqueous environments at Endeavour Crater, Mars. Science 343 (6169). http://dx.doi.org/10.1126/science.1248097.

Bibring, J.-P., et al., 2006. Global mineralogical and aqueous Mars history derived from OMEGA/Mars express data. Science 312, 400–404.

Bishop, J.L., Pieters, C.M., Edwards, J.O., 1994. Infrared spectroscopic analyses on the nature of water in montmorillonite. Clays Clay Miner. 42, 702–716.

Bishop, J.L., Murad, E., Madejova, J., Komadel, P., Wagner, U., Scheinost, A., 1999. Visible, Mössbauer and infrared spectroscopy of dioctahedral smectites: structural analyses of the Fe-bearing smectites Sampor, SWy-1 and SWa-1. In: Komada, H., Mermut, A.R., Torrance, J.K. (Eds.), Clay Minerals for Our Future. Proceedings of the 11th International Clay Conference. Ottawa, June 1997, pp. 413–419.

Bishop, J., Madejova, J., Komadel, P., Froschl, H., 2002a. The influence of structural Fe, Al and Mg on the infrared OH bands in spectra of dioctahedral smectites. Clay Miner. 37, 607–616.

Bishop, J., Murad, E., Dyar, M.D., 2002b. The influence of octahedral and tetrahedral cation substitution on the structure of smectites and serpentines as observed through infrared spectroscopy. Clay Miner. 37, 617–628.

Bishop, J.L., Dobrea, E.Z.N., McKeown, N.K., Parente, M., Ehlmann, B.L., Michalski, J.R., Milliken, R.E., Poulet, F., Swayze, G.A., Mustard, J.F., Murchie, S.L., Bibring, J.P., 2008. Phyllosilicate diversity and past aqueous activity revealed at Mawrth Vallis, Mars. Science 321, 830–833.

Bishop, J.L., Tirsch, D., Tornabene, L.L., Jaumann, R., McEwen, A.S., McGuire, P.C., Ody, A., Poulet, F., Clark, R.N., Parente, M., Voigt, J., Aydin, Z., Bamberg, M., Petau, A., McKeown, N.K., Mustard, J.F., Hash, C., Murchie, S.L., Swayze, G., Neukum, G., Seelos, F., 2013. Mineralogy and morphology of geologic units at Libya Montes, Mars: ancient aqueous outcrops, mafic flows, fluvial features and impacts. J. Geophys. Res. 118. http://dx.doi.org/10.1029/2012JE004151.

Boynton, W.V., Taylor, G.J., Karunatillake, S., Reedy, R.C., Keller, M., 2008. Elemental abundances determined via the Mars Odyssey GRS. In: Bell, J. (Ed.), The Martian Surface, pp. 105–124.

Bristow, T., Milliken, R.E., 2011. A terrestrial perspective on authigenic clay production in ancient Martian lakes. Clays Clay Miner. 59 (4), 339–358.

Burns, R.G., 1993. Rates and mechanisms of chemical-weathering of ferromagnesian silicate minerals on Mars. Geochim. Cosmochim. Acta 57, 4555–4574.

Carter, J., Poulet, F., Bibring, J.P., Mangold, N., Murchie, S., 2013. Hydrous minerals on Mars as seen by the CRISM and OMEGA imaging spectrometers: updated global view. J. Geophys. Res., Planets 118, 831–858.

Changela, H.G., Bridges, J.C., 2010. Alteration assemblages in the nakhlites: variation with depth on Mars. Meteorit. Planet. Sci. 45, 1847–1867.

Christensen, P.R., et al., 2001. Mars global surveyor thermal emission spectrometer experiment: investigation description and surface science results. J. Geophys. Res., Planets 106, 23823–23871.

Cuadros, J., Dekov, V.M., Fiore, S., 2008. Crystal chemistry of the mixed-layer sequence talc–talc–smectite–smectite from submarine hydrothermal vents. Am. Mineral. 93, 1338–1348.

Cuadros, J., 2010. Crystal-chemistry of mixed-layer clay minerals in interstratified clay minerals. In: Fiore, S., Cuadros, J., Huertas, F.J. (Eds.), AIPEA Education Series (Pub. 1), pp. 11–33.

Cuadros, J., Michalski, J., Dekov, V., Bishop, J.L., Fiore, S., Darby Dyar, M., 2013. Crystal-chemistry of interstratified Mg/Fe-clay minerals from seafloor hydrothermal sites. Chem. Geol. 360–361, 142–158.

Cuadros, J., Michalski, J., Dekov, V., Bishop, J.L., in review. Octahedral chemistry of 2:1 clay minerals and hydroxyl band position in the near-infrared. Applications to Mars. American Min.

Deocampo, D.M., Cuadros, J., Wing-Dudek, T., Olives, J., Amouric, M., 2009. Saline lake diagenesis as revealed by coupled mineralogy and geochemistry of multiple ultrafine clay phases: Pliocene Olduvai gorge, Tanzania. Am. J. Sci. 309, 834–868. http://dx.doi.org/10.2475/09.2009.03.

Drits, V.A., Dainyak, L.G., Muller, F., Besson, G., Manceau, A., 1997. Isomorphous cation distribution in celadonites, glauconites, and Fe-illites determined by infrared, Mössbauer and EXAFS spectroscopies. Clay Miner. 32, 153–179.

Ehlmann, B.L., Mustard, J.F., Murchie, S.L., Bibring, J.P., Meunier, A., Fraeman, A.A., Langevin, Y., 2011. Subsurface water and clay mineral formation during the early history of Mars. Nature 479, 53–60.

Ehlmann, B.L., Mustard, J.F., Swayze, G.A., Clark, R.N., Bishop, J.L., Poulet, F., Marais, D.J.D., Roach, L.H., Milliken, R.E., Wray, J.J., Barnouin-Jha, O., Murchie, S.L., 2009. Identification of hydrated silicate minerals on Mars using MRO-CRISM: geologic context near Nili Fossae and implications for aqueous alteration. J. Geophys. Res., Planets 114.

Ehlmann, B.L., Mustard, J.F., Murchie, S.L., Poulet, F., Bishop, J.L., Brown, A.J., Calvin, W.M., Clark, R.N., Des Marais, D.J., Milliken, R.E., Roach, L.H., Roush, T.L., Swayze, G.A., Wray, J.J., 2008. Orbital identification of carbonate-bearing rocks on Mars. Science 322, 1828–1832.

Fairén, A.G., Chevrier, V., Abramov, O., Marzo, G.A., Gavin, P., Davila, A.F., Tornabene, L.L., Bishop, J.L., Roush, T.L., Gross, C., Kneissl, T., Uceda, E.R., Dohm, J.M., Schulze-Makuch, D., Rodriguez, J.A.P., Amils, R., McKay, C.P., 2010. Noachian and more recent phyllosilicates in impact craters on Mars. Proc. Natl. Acad. Sci. USA 107, 12095–12100.

Farmer, V.C., 1974. The layer silicates. In: Farmer, V.C. (Ed.), The Infrared Spectra of Minerals. Mineralogical Society, London, pp. 331–363.

Gates, W.P., 2005. Infrared spectroscopy and the chemistry of dioctahedral smectites. In: Kloprogge, T. (Ed.), The Application of Vibrational Spectroscopy to Clay Minerals and Layered Double Hydroxides. In: Clay Minerals Society Workshop Lectures, vol. 13. Aurora, USA, pp. 41–64.

Gaudin, A., Dehouck, E., Mangold, N., 2011. Evidence for weathering on early Mars from a comparison with terrestrial weathering profiles. Icarus 216, 257–268.

Grauby, O., Petit, Sabine, Decarreau, A., Baronnet, A., 1994. The nontronite–a saponite series: an experimental approach. Eur. J. Mineral. 6, 99–112.

Hicks, L.J., Bridges, J.C., Gurman, S.J., 2014. Ferric saponite and serpentine in the nakhlite martian meteorites. Geochim. Cosmochim. Acta 136, 194–210.

Madejová, J., Komadel, P., Čičel, B., 1994. Infrared study of octahedral site populations in smectites. Clay Miner. 29, 319–326.

McSween, H.Y., Taylor, G.J., Wyatt, M.B., 2009. Elemental composition of the Martian crust. Science 324, 736–739.

Meunier, A., Petit, S., Ehlmann, B.L., Dudoignon, P., Westall, F., Mas, A., El Albani, A., Ferrage, E., 2012. Magmatic precipitation as a possible origin of Noachian clay minerals on Mars. Nat. Geosci. 5, 739–743. http://dx.doi.org/10.1038/NGEO1572.

Meyer, C., 2012. The martian meteorite compendium. NASA JSC Astromaterials Research & Exploration Science (ARES).

Michalski, J.R., Poulet, F., Bibring, J.-P., Mangold, N., 2010. Analysis of phyllosilicate deposits in the Nili Fossae region of Mars: comparison of TES and OMEGA data. Icarus 206, 269–289.

Milliken, R.E., Fischer, W.W., Hurowitz, J.A., 2009. Missing salts on early Mars. Geophys. Res. Lett. 36, L11202. http://dx.doi.org/10.1029/2009GL038558.

Milliken, R.E., Bish, D., Bristow, T., Mustard, J.F., 2010. The case for mixed-layer clay minerals on Mars. In: 41st LPSC Conference. Houston, USA. Abstract 1 #2030.

Murchie, S.L., et al., 2009. A synthesis of Martian aqueous mineralogy after 1 Mars year of observations from the Mars Reconnaissance Orbiter. J. Geophys. Res., Planets 114.

Niles, P.B., Catling, D.C., Berger, G., Chassefiere, E., Ehlmann, B.L., Michalski, J.R., Morris, R., Ruff, S.W., Sutter, B., 2013. Geochemistry of carbonates on Mars: implications for climate history and nature of aqueous environments. Space Sci. Rev. 174, 301–328.

Noe Dobrea, E.Z., et al., 2010. Mineralogy and stratigraphy of phyllosilicate-bearing and dark mantling units in the greater Mawrth Vallis/west Arabia Terra area: constraints on geological origin. J. Geophys. Res., Planets 115.

Osterloo, M.M., Anderson, F.S., Hamilton, V.E., Hynek, B.M., 2010. Geologic context of proposed chloride-bearing materials on Mars. J. Geophys. Res., Planets 115, E10012. http://dx.doi.org/10.1029/2010JE003613.

Perdikatsis, B., Burzlaff, H., 1981. Z. Kristallogr. 156, 177–186.

Petit, S., Decarreau, A., Martin, F., Buchet, R., 2004. Refined relationship between the position of the fundamental OH stretching and the first overtones for clay minerals. Phys. Chem. Miner. 31, 585–592.

Petit, S., 2005. Crystal-chemistry of talcs: a NIR and MIR spectroscopic approach in the application of vibrational spectroscopy to clay minerals and layered double hydroxides. In: Kloprogge, T. (Ed.), Clay Minerals Society Workshop Lectures, vol. 13. Aurora, USA, pp. 41–64.

Poulet, F., Bibring, J.P., Mustard, J.F., Gendrin, A., Mangold, N., Langevin, Y., Arvidson, R., Gondet, B., Gomez, C., 2005. Phyllosilicates on Mars and implications for early martian climate. Nature 438, 623–627.

Poulet, F., Gomez, C., Bibring, J.P., Langevin, Y., Gondet, B., Pinet, P., Belluci, G., Mustard, J., 2007. Martian surface mineralogy from observatoire pour la mineralogie, l'Eau, les Glaces et l'Activite on board the Mars express spacecraft (OMEGA/MEx): global mineral maps. J. Geophys. Res., Planets 112.

Stolper, E.M., et al., 2013. The petrochemistry of Jake_M: a martian mugearite. Science 342, 1239463.

Tanaka, K.L., Skinner, J.A., Dohm J.M., Irwin III, R.P., Kolb, E.J., Fortezzo, C.M., Platz, T., Michael, G.G., Hare, T.M., 2014. Geologic Map of Mars. 1:20,000,000 scale. USGS, Scientific Investigations Map 3292.

Treiman, A.H., et al., 2014. Ferrian saponite from the Santa Monica Mountains (California, U.S.A., Earth): characterization as an analog for clay minerals on Mars with application to Yellowknife Bay in Gale Crater. Am. Mineral. 99, 2234–2250.

Vaniman, D.T., et al., 2013. Mineralogy of a mudstone on Mars. Science. http://dx.doi.org/10.1126/science.1243480.

Wilkins, R., Ito, J., 1967. Infrared spectra of some synthetic talcs. Am. Mineral. 52, 1649–1661.